THE JOURNAL OF PHYSICAL CHEMISTRY C

Article

pubs.acs.org/JPCC

Tuning the Geometrical and Crystallographic Characteristics of Bi_2Te_3 Nanowires by Electrodeposition in Ion-Track Membranes

Oliver Picht,*[,†] Sven Müller,[†] Ina Alber,[†] Markus Rauber,[†,‡] Jessica Lensch-Falk,[§] Douglas L. Medlin,[§] Reinhard Neumann,[†] and Maria Eugenia Toimil-Molares*[,†]

[†]GSI Helmholtz Centre for Heavy Ion Research GmbH, Planckstrasse 1, D-64291 Darmstadt, Germany

[‡]Technical University Darmstadt, Department of Material- and Geosciences, Petersenstrasse 23, D-64827 Darmstadt, Germany

[§]Sandia National Laboratories, Livermore, California 94551, United States

ABSTRACT: We report the fabrication of Bi_2Te_3 nanowires with diameters as small as 15 nm, which is comparable to the size theoretically estimated for the onset of improvement of the thermoelectric figure of merit *ZT* by quantum-size effects. The versatility of the template-assisted growth, combining self-prepared ion-track etched membranes and electrochemical deposition, has been employed to synthesize Bi_2Te_3 nanowires with controlled diameters in 10, 30, and 60 μm thick membranes and with large aspect ratios (length over diameter) of up to 1000. SEM, HRTEM, and XRD investigations reveal how morphology, surface roughness, and crystalline orientation of the Bi_2Te_3 nanowires depend on deposition potential, temperature, and channel diameter.

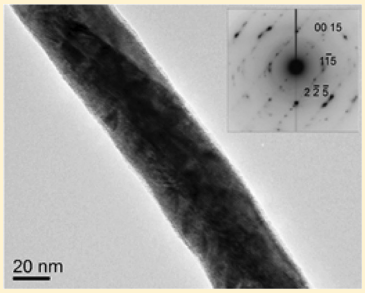

INTRODUCTION

Tuning the thermal and electrical properties of bulk materials via alloying and doping has been the most common approach to raise their thermoelectric (TE) figure of merit *ZT*, and thus to improve the device performance.[1] However, the increase attained appears to be limited. Theoretical calculations in the early 90s by Hicks and Dresselhaus[2,3] proposed a very promising route to bypass classical limitations on *ZT*, which is described by $Z{\cdot}T = (S^2\sigma/\kappa){\cdot}T$. The power factor ($S^2\sigma$), given by the Seebeck coefficient (S) and the electrical conductivity (σ), can be selectively increased via quantum-size effects, while the thermal conductivity (κ) can be lowered through enhanced phonon scattering. Theoretical investigations of the TE properties of Bi_2Te_3 nanostructures[2−8] predict a significant improvement of *ZT* for wires with diameters below 30 nm. The beneficial impact of low dimensionality on thermoelectric properties has already been demonstrated experimentally on superlattices[9] and nanostructured bulk Bi_2Te_3-based materials.[10−14] Measurements on nanowires have been scarcer due to (i) the technological challenge of measuring the absolute values of S, σ, and κ of individual nanowires and (ii) the difficulty of synthesizing Bi_2Te_3 nanowires with the desired geometrical and compositional characteristics, and subsequently handling them while maintaining their chemical and mechanical stability. Despite these difficulties, promising results have been presented recently for single Bi_2Te_3 nanowires[15,16] as well as for Si nanowires with varying surface roughness.[17,18] In addition, the thermal diffusivity of Bi_2Te_3 nanowire arrays embedded in anodized alumina (AAO) membranes had been previously reported.[19] More recently, Biswas et al. reported the thermal conductance of bismuth telluride nanowire arrays in AAO and demonstrated the minimization of the parasitic thermal conductance by replacing the AAO matrix with the epoxy SU8.[20]

A variety of different approaches have been pursued for the fabrication of bismuth telluride based nanostructures and nanostructured material.[10−14,21,22] Methods for the preparation of bismuth telluride based nanowires include the solvothermal synthesis of nanorods,[23−25] the On-Film growth technique,[26] and the template-assisted electrochemical deposition.[27−37,40,41] Among these techniques, the latter one potentially enables the tuning of geometrical, morphological, and crystallographic properties of nanowires with the largest control and in an independent manner. However, to our knowledge, most works to date have reported the growth of bismuth telluride wires with diameters larger than 40 nm and only few address the impact of nanoporous membranes, nanochannel diameter, or deposition conditions on the preferential crystalline orientation of the nanowire arrays. Moreover, AAO membranes have been by far the most commonly used templates for the electrochemical deposition of Bi_2Te_3 nanowires, and only very few experimental investigations have employed polymeric membranes. For example, 60 nm diameter $(Bi_{1-x}Sb_x)_2Te_3$ wires were grown in commercially available polycarbonate membranes (thickness 6 μm),[37] the wires displaying the so-called cigar-like shape of the hosting pores.[38,39] Additional works by Koukharenko et al.[40] and Frantz et al.[41] reported the growth of 80 nm diameter Bi_2Te_3 nanowires in 20 μm thick polyimide (Kapton HN) and 60 nm diameter wires in 30 μm thick polycarbonate membranes (Makrofol N), respectively.

Received: November 1, 2011
Revised: January 20, 2012
Published: February 28, 2012

dx.doi.org/10.1021/jp210491g | *J. Phys. Chem. C* 2012, 116, 5367−5375

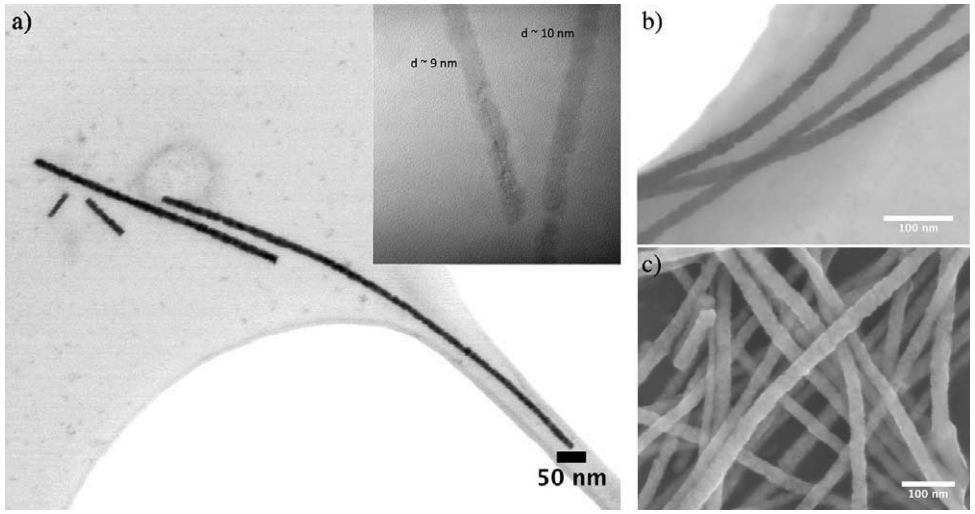

Figure 1. SEM images of nanowires grown in 10 μm thick polycarbonate membranes. Average nanowire diameters are (a) 14, (b) 19, and (c) 24 nm. The inset in (a) shows a TEM image of nanowire sections with diameters of approximately 9 and 10 nm.

In this work, we explore the use of polymeric membranes for growth of Bi_2Te_3 nanowires in further detail. We demonstrate that, by simultaneous tuning of all fabrication parameters, electrodeposition in polymeric membranes can be optimized to synthesize nanowires with sets of geometrical and crystallographic characteristics particulary interesting for both basic investigations of low-dimensional Bi_2Te_3 nanomaterials (diameters below 20 nm,[3,4,6−8] controlled morphology,[8] and crystallographic structure[6]), as well as for thermoelectric model systems and devices[42,43] (long wires to achieve and maintain a large enough temperature gradient, and possible integration to devices). Self-fabricated etched ion-track membranes are prepared from polycarbonate foils with a very low thermal conductivity of approximately 0.2 W/mK,[44] offering an adjustable number density of cylindrical nanochannels. Combining direct electrodeposition and ion-track technology, we report the fabrication of Bi_2Te_3 nanowires with diameters from 150 nm down to 10 nm, and lengths of up to 60 μm. Our study shows how the parameters involved in the electrodeposition process influence the morphology, the crystallinity, and the preferred crystallographic orientation of nanowires with various diameters and lengths interesting for both basic research on TE nanomaterials and TE devices.

EXPERIMENTAL METHODS

Etched ion-track membranes are fabricated by irradiation of polycarbonate (PC) foils (10 μm thick Makrofol KG and 30 and 60 μm thick Makrofol N, Bayer) with Au and U ions (energy, 5.9 and 11.1 MeV/u; fluence, 10^8−5×10^9 ions/cm^2) at the linear accelerator (UNILAC) of the GSI Helmholtz Centre for Heavy Ion Research. Symmetrical chemical etching of the ion tracks in 6 mol/L NaOH at T = 50 °C yields membranes with practically parallel and cylindrical pores and aspect ratios up to 1000.[45] The nanochannel diameter increases linearly with etching time.[45] Nanowire arrays are grown potentiostatically with a Gamry REF600 potentiostat in a thermostated three-electrode setup with a gold cathode (thin layer sputtered onto one side of the membrane with an Edwards S150 B sputter coater prior to deposition), a Pt counter electrode, and a saturated calomel reference electrode (SCE). The applied potentials U were 0 and −100 mV vs SCE. In addition, two temperatures, 4 and 20 °C, were selected for electrodeposition. The constituents of the electrolyte were chosen as described by Magri et al.;[46] the ion concentration was adjusted to obtain an aqueous solution consisting of 5 mmol/L bismuth nitrate pentahydrate (98%, Alfa Aesar) and 7.5 mmol/L TeO_2 (99.5+%, Merck KGaA) in 1 mol/L nitric acid. For a comparative measurement, a Bi-rich electrolyte was prepared with 10 mmol/L bismuth nitrate pentahydrate, 5 mmol/L TeO_2, and 1 mol/L nitric acid.

For the analysis of nanowires and membranes, scanning electron microscopy (SEM) was conducted with a JEOL JSM-7401F electron microscope in the classical mode of operation (detection of secondary and backscattered electrons), as well as in transmission mode (STEM-in-SEM). The crystallinity of single nanowires was further investigated by high-resolution transmission electron microscopy (HRTEM) with a 400 kV JEOL 4000EX, and a 200 kV JEOL 2010F. For TEM and STEM-in-SEM investigations, a small piece of the nanowire−polymer composite was immersed in dimethylformamide or dichloromethane, and the nanowires were then transferred onto a TEM grid via drop-casting. X-ray diffraction analysis (XRD) on nanowire arrays was performed with Cu Kα radiation of a Seifert X-ray generator and a HZG-4 four-circle goniometer. Measurements were conducted in reflection geometry to determine the lattice planes parallel to the template surface, that is, perpendicular to the wire axis. For analysis of the preferential crystalline orientation of the arrays, the growth process was stopped before an onset of overgrowth was evident in the deposition curves. To avoid overlap of reflections from the substrate or sample holder with signals from the Bi_2Te_3 arrays, the Au cathode was removed by means of a KI/I_2 solution prior to diffraction analysis.

RESULTS AND DISCUSSION

In this section, we describe how specific templates can be designed to fabricate nanowires with controlled diameters and lengths. We explore the observed dependence between wire morphology and electrodeposition temperature and potential and discuss in detail the microstructure of the wires, as investigated by TEM, and the preferred crystallographic orientation, as studied by XRD, on nanowires with different sizes.

Controlled Growth of Nanowires with Very Small Diameters. Wire diameter is one of the crucial parameters for

dx.doi.org/10.1021/jp210491g | J. Phys. Chem. C 2012, 116, 5367−5375

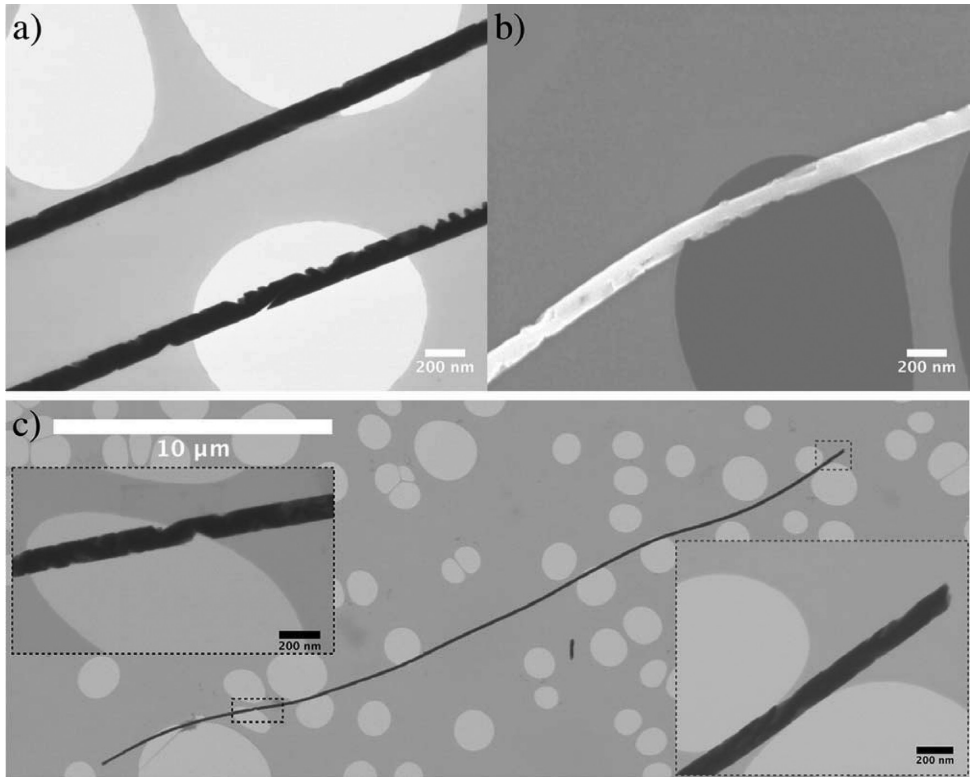

Figure 2. STEM-in-SEM images of nanowires with larger surface roughness fabricated at −100 mV vs SCE in 30 μm thick templates with a nanochannel diameter of 120 nm at (a) 20 °C and (b) 4 °C, as well as in (c) 60 μm thick templates.

the enhancement of *ZT* by quantum-size effects and phonon scattering.[3,7,8,17−19] Figure 1 displays an overview of single nanowires and bundles prepared in 10 μm thick PC templates. By etching the polymer foils for short times between 40 and 60 s, templates with very small pores were fabricated. After electrochemical deposition in the resulting nanopores and subsequent dissolution of the membrane, a linear dependence between nanowire diameter and etching time was determined. In Figure 1, Bi_2Te_3 wires with average diameters of 14 ± 3 nm (Figure 1a), 19 ± 2 nm (Figure 1b), and 24 ± 3 nm (Figure 1c) are shown. Both SEM and TEM measurements revealed wire segments with diameters as small as 9 nm (Figure 1a, inset). This demonstrates that nanowires with diameters in the few-nanometer range, for which quantum-size effects are predicted, can be efficiently fabricated by electrochemical methods in 10 μm thick PC membranes.

Morphology of the Nanowires as a Function of the Deposition Parameters. In addition to diameter, morphology and surface roughness are also expected to influence electron and phonon scattering, as well as the mechanical and thermal stability of the nanostructure.[8,17,18,47] Using the template method, we systematically investigated the influence of the relevant parameters (pore diameter, deposition temperature, and deposition potential) on the morphology of the nanowires grown in ion-track etched PC membranes. For this, we prepared 30 μm thick PC templates with pore diameters between 25 and 120 nm by adjusting the etching times from 60 s to 6 min. Electrodeposition was conducted at both 20 and 4 °C, applying potentials of −100 and 0 mV vs SCE under thermostated conditions. Figure 2 shows STEM-in-SEM images of Bi_2Te_3 nanowires grown at −100 mV vs SCE at 20 (Figure 2a) and 4 °C (Figure 2b) with average nanowire diameters of 120 nm. All wires exhibited a pronounced surface roughness, which is visible as dents and constrictions of various widths, and thickness-related changes in the absorption of the electron beam in the SEM. The STEM-in-SEM images of a 29 μm long nanowire, electrodeposited in a 60 μm thick membrane, at 4 °C and −100 mV, are shown in Figure 2c. The wire also exhibits pronounced diameter constrictions at various points, and changes in electron beam transmission along the wire are visible. An enlarged view of two regions (separated by approximately 22 μm) is presented in the insets. The respective diameters at these positions are roughly 120 and 130 nm. At the smaller end of the wire, the tip diameter is approximately 100 nm. Keeping in mind that the templates are prepared by symmetrical etching from two sides, these results show that wires with small diameter variations can be successfully prepared in thicker ion-track etched templates.

A comparison of the images a and b in Figure 2 shows that a reduction of the deposition temperature from 20 to 4 °C has no significant impact on the nanowire morphology, even though the growth process is slowed significantly, namely, by approximately 40−50%. The maximum growth rate is estimated by the time needed for the complete filling of the first pores, which is visible as an increase in the deposition current during fabrication.[48] Similar reduction of the growth rate (5.5 to 2.7 μm/h) was reported for electrodeposition of Bi_2Te_3 nanowires in AAO membranes by Trahey et al.[34] The change from 30 to 60 μm thick membranes also shows no significant impact on the surface morphology (Figure 2c). However, a strong influence of deposition potential on nanowire morphology is evidenced by comparison of Figures 2 and 3. Figure 3 shows SEM images of nanowires deposited in 30 μm membranes with pores with similar diameters of 110−120 nm at 0 mV vs SCE at both 20 °C (Figure 3a) and 4 °C (Figure 3b). In addition, nanowires deposited under identical conditions in a 60 μm

dx.doi.org/10.1021/jp210491g | *J. Phys. Chem. C* 2012, 116, 5367−5375

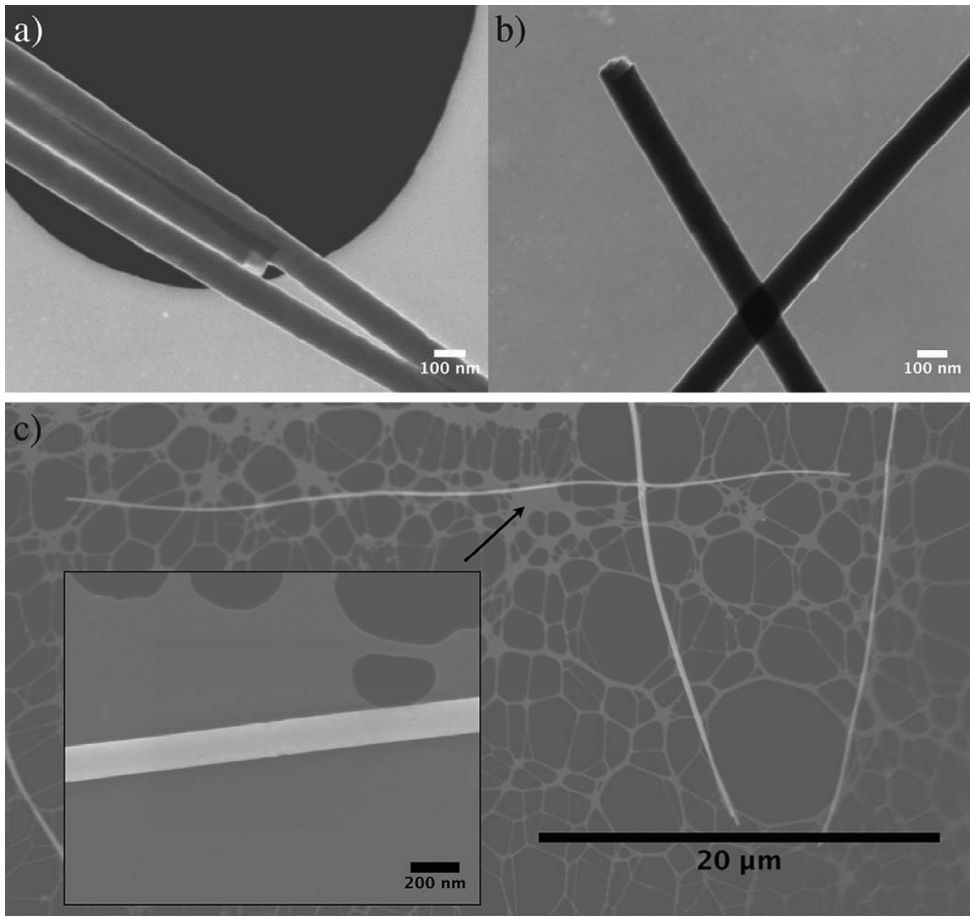

Figure 3. STEM-in-SEM images of nanowires with smoother surface contours fabricated at 0 mV vs SCE in 30 μm thick templates with nanochannel diameters of ~120 nm at (a) 20 °C and (b) 4 °C, as well as (c) in 60 μm thick templates with pore diameters of ~140 nm at 20 °C.

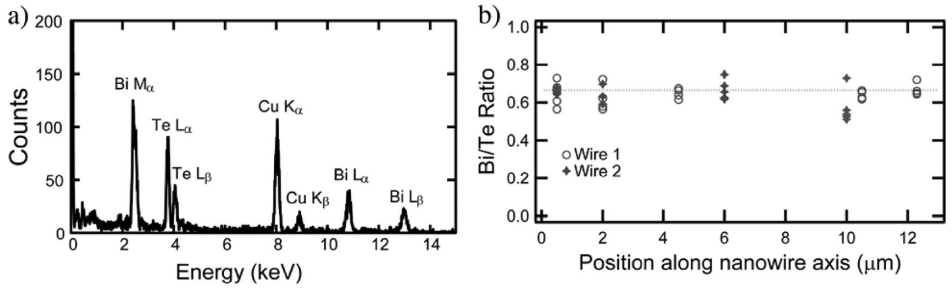

Figure 4. (a) A representative STEM/EDS spectrum collected from a Bi_2Te_3 nanowire is shown. (b) The ratio of atomic fraction of Bi to Te along the length of two nanowires deposited at 0 mV vs SCE and 4 °C is shown to demonstrate the compositional homogeneity along the length of the nanowires.

template are included for comparison (Figure 3c). All wires exhibit smoother surface contours than their counterparts deposited with −100 mV vs SCE.

Variations of the transmitted electron beam intensity are visible at positions of nanowire overlap, and only a few sharp edges and constrictions were found along the wires electrodeposited in 30 and 60 μm membranes. For thinner wires with diameters of the order of 50 nm, a similar dependence of surface roughness on deposition potential and temperature was observed in most cases. No clear determination of the surface contour modification by variation of the deposition potential was possible for nanowires with diameters < 40 nm.

Investigation of Compositional Uniformity by STEM-EDS. Because of the important influence of the Bi and Te concentration on ZT of Bi_2Te_3,[49] we wanted to confirm that our deposition conditions yield a nanowire composition that is close to stoichiometric Bi_2Te_3 and that the nanowires are compositionally homogeneous along their lengths. STEM-EDS indicates that these nanowires grown at 0 and −100 mV vs SCE are consistent with Bi_2Te_3. Figure 4a shows a representative EDS spectrum collected in STEM mode from a nanowire deposited at 0 mV vs SCE at 4 °C, the Bi M and L lines and Te L lines are clearly observed. The Cu K lines are present as a result of the high Cu background from the Cu support grid. For two arbitrary nanowires, the determined Bi/Te ratios are presented in Figure 4b and plotted with respect to the measurement positions along the nanowires, demonstrating

dx.doi.org/10.1021/jp210491g | J. Phys. Chem. C 2012, 116, 5367−5375

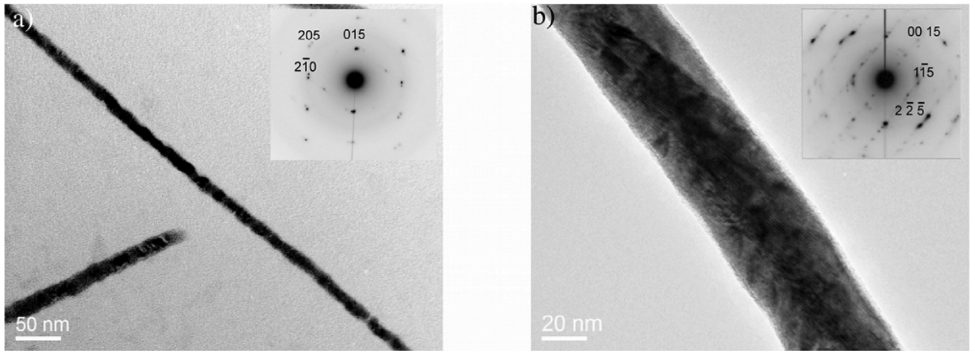

Figure 5. TEM and electron diffraction from segments of polycrystalline nanowires with diameters of (a) 13 and 17 nm and (b) 44 nm. The nanowires were grown at 0 mV vs SCE and 4 °C in (a) 10 and (b) 30 μm thick membranes. Electron diffraction shows {205}-type planes oriented perpendicular to the wire axis (the (205) and (2$\bar{2}$5) planes are both in the equivalent {205} family of planes).

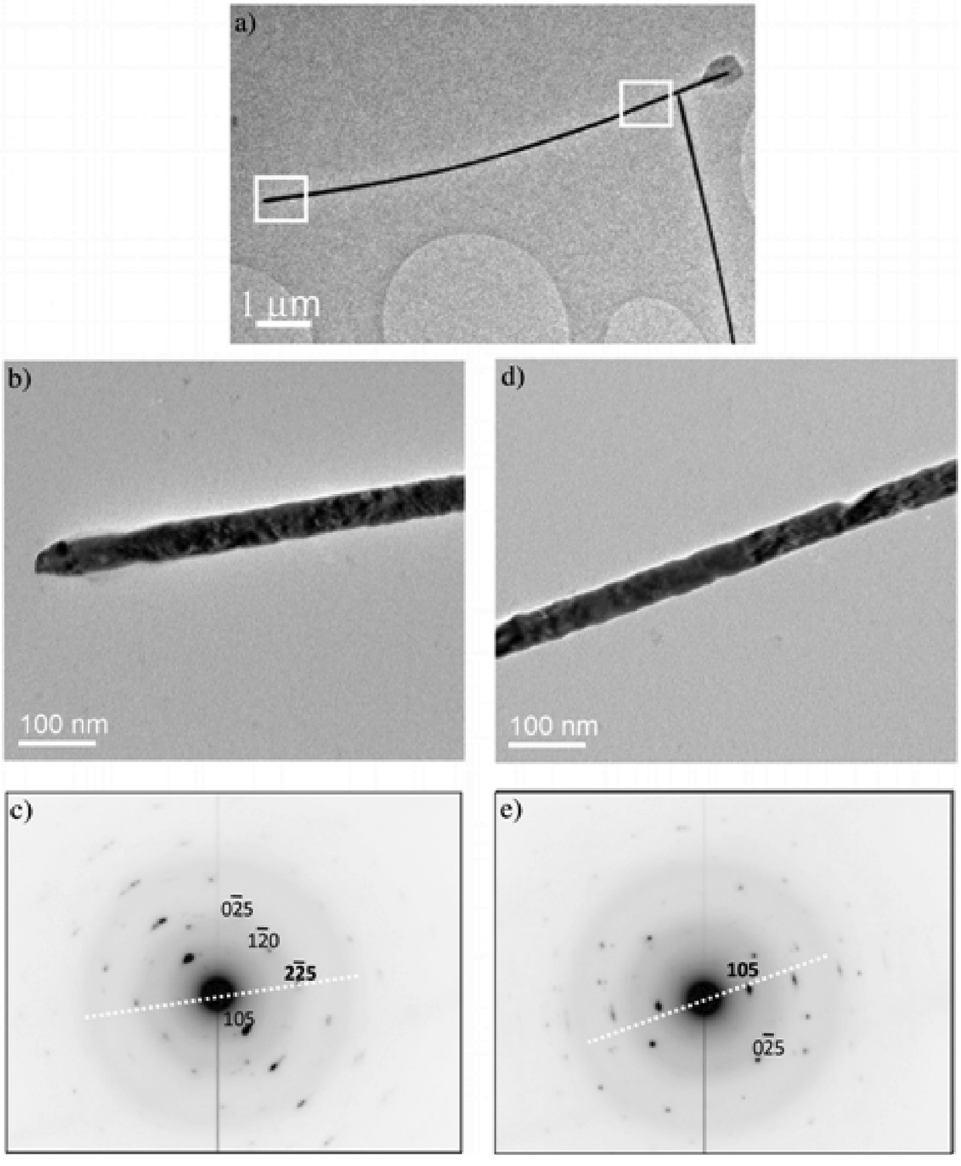

Figure 6. (a) TEM image of a representative nanowire grown at 4 °C and −100 mV vs SCE. (b, d) TEM images displaying the polycrystalline wire structure and surface dents along the nanowire surface. (c, e) Electron diffraction patterns corresponding to the images in (b) and (d).

that both nanowires have an appropriate Bi/Te ratio for Bi_2Te_3 and that the composition does not vary systematically along the nanowire axis.

Investigation of the Nanowire Crystallinity by TEM. Besides wire diameter, morphology, and composition, two additional factors strongly influence the thermoelectric properties of

dx.doi.org/10.1021/jp210491g | J. Phys. Chem. C 2012, 116, 5367−5375

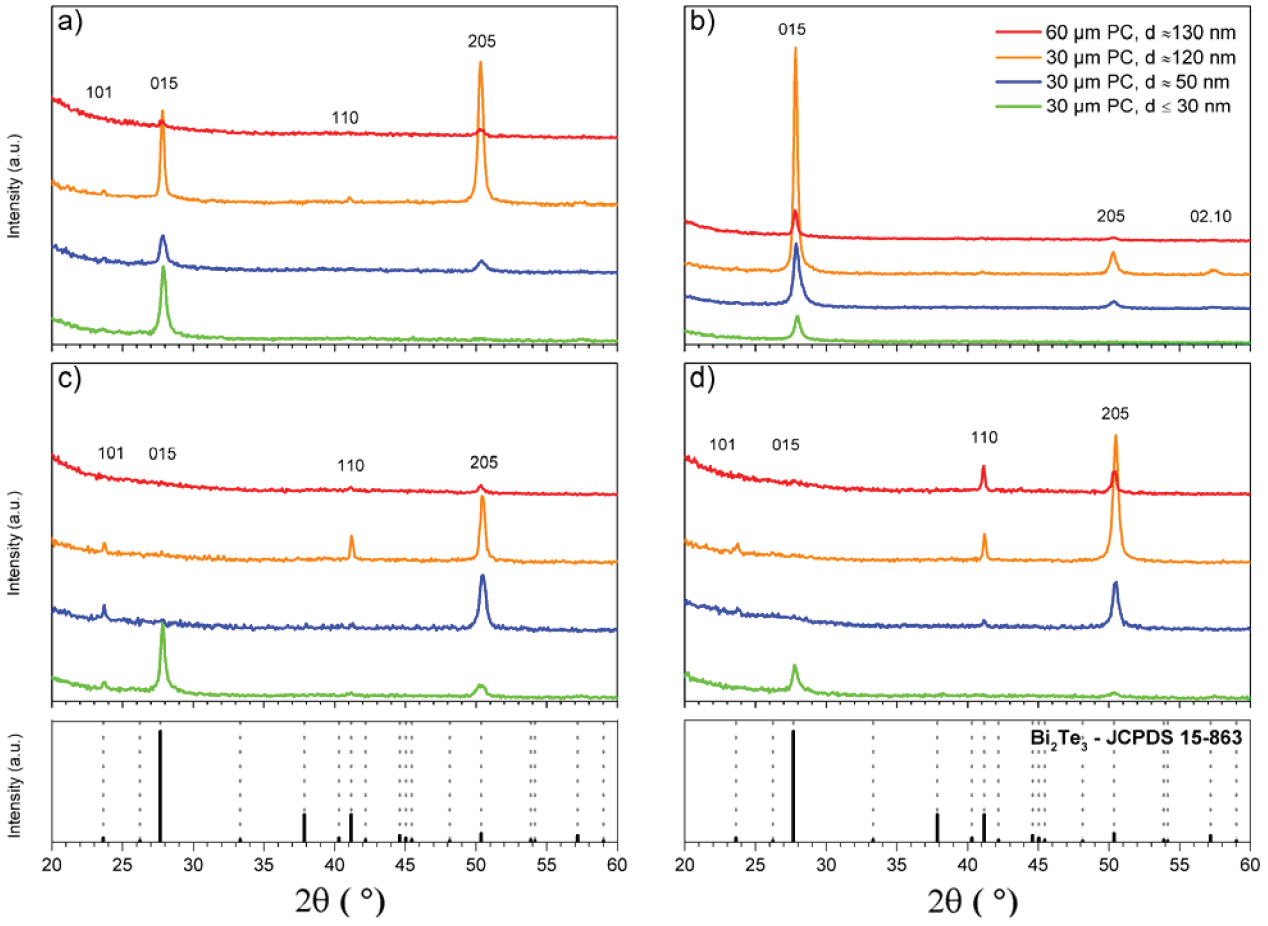

Figure 7. Four sets of X-ray diffractograms of Bi_2Te_3 nanowires with diameters of 130, 120, 50, and ≤30 nm embedded in 30 μm (green, blue, and orange lines) and 60 μm (red line) membranes. Standard powder diffraction data are shown at the bottom. Within each set of diffractograms, all samples are fabricated with the same deposition potential, temperature, and time. Parameters for the electrochemical growth were (a) −100 mV vs SCE and 20 °C, (b) −100 mV vs SCE and 4 °C, (c) 0 mV vs SCE and 20 °C, and (d) 0 mV vs SCE and 4 °C.

nanowires, namely, crystallinity and crystallographic orientation. The crystal symmetry of Bi_2Te_3 is given by the rhombohedral space group $R\bar{3}m$.[50,51] In the literature, Bi_2Te_3 is often described by a hexagonal unit cell consisting of three quintets of alternating Te and Bi layers stacked along the c axis, with reported lattice parameters close to a = 4.38 Å and c = 30.5 Å.[50−52] Because of its highly anisotropic crystalline structure, the thermoelectric properties of Bi_2Te_3 and other bismuth compounds are known to depend strongly on crystallographic orientation.[49,53−55] As demonstrated, for example, in the case of Bi, Cu, and Au nanowires, grain size and nanowire diameter can significantly influence the electrical conductivity.[56−58]

By TEM, we investigated the grain structure and orientation of nanowires with small diameters (<50 nm) prepared under various deposition conditions. In all of our measurements, we found polycrystalline microstructures with grains that could be indexed to the expected Bi_2Te_3 crystal structure. However, we did note some changes in preferential orientation with the deposition potential. We first consider the nanowires deposited at 0 mV vs SCE and 4 °C, in both 10 and 30 μm thick templates (Figure 5). As illustrated by the two electron diffraction (ED) patterns collected from these wires (Figure 5, insets), we commonly find grains that are oriented with {205}-type planes perpendicular to the wire axis (note: (205) and $(2\bar{2}\bar{5})$ are equivalent, both falling in the {205} family of planes).

In comparison, TEM and ED measurements of nanowires of a similar diameter (50 nm) deposited at −100 mV vs SCE and at 4 °C indicate that both {015} and {205} planes are found to be perpendicular to the wire axis, as shown in Figure 6. The results for deposition at 0 mV, as well as −100 mV vs SCE, are consistent with the XRD results on embedded nanowire arrays, as described below. Furthermore, the TEM images (Figure 6b,d) and their corresponding electron diffraction patterns (Figure 6c,e, respectively) reveal that both orientations can be present within an individual nanowire.

The crystallinity of the nanowires was investigated by dark-field TEM and ED for nanowires grown at both 0 and −100 mV vs SCE. In both cases, nanowires are polycrystalline, with grain sizes ranging from 10 nm to larger than 100 nm. This indicates that, for the employed deposition conditions, the variation in the applied potential does not affect the crystallinity and grain size. However, as indicated by the representative ED patterns in Figures 5 and 6, the preferential orientation of the nanowires does vary when increasing or decreasing the potential.

Investigation of the Preferred Crystallographic Orientation of Wire Arrays as a Function of Nanopore Size and Deposition Conditions. To complement the information obtained by TEM on individual nanowires, the preferential crystallographic orientation of different arrays (area ~ 1 cm^2) of nanowires with various diameters was investigated by 4-circle

dx.doi.org/10.1021/jp210491g | J. Phys. Chem. C 2012, 116, 5367−5375

X-ray diffractometry. The geometrical arrangement of the XRD studies on nanowire arrays embedded in the polymer membrane provides information of the average preferred orientation of the crystals along the wire axis.

To investigate as well the influence of the *membrane thickness* on the crystal growth, we fabricated 60 μm thick polycarbonate membranes with channel diameters of approximately 130 nm, choosing the same nominal fluence (10^8 cm^{-2}) and same deposition conditions (electrolyte, voltage, temperature, and deposition times) as for the thicker nanowires grown in 30 μm templates. Under the same deposition conditions, currents measured in 60 μm membranes were significantly lower than those in the 30 μm counterparts. Thus, for identical deposition times, the measured charge (ideally correlated with the mass by Faraday's law) during the growth in 60 μm thick templates was less than 50% of the measured value for growth in 30 μm membranes. The smaller amount of material deposited inside the 60 μm long nanochannels led to reduced peak intensities, even for an identical preferential crystallographic orientation of the nanowires.

The ω-2θ scans shown in Figure 7 indicate that the nanowire arrays are strongly textured for each sample. Additionally, they elucidate the dependence of nanowire orientation on nanowire diameter, temperature, and deposition potential.

In general, two main reflections are visible in the diffractograms of Figure 7a, originating from X-ray diffraction at the {015} and {205} planes of Bi_2Te_3. In the case of large wire diameters (120 nm), small 110 and 02.10 reflections are also visible. The intensity $I(hkl)$ of these reflections and the absence of other orientations with similar or higher intensity than the 205 peak (i.e., reflections from {006}, {10.10}, {00.15}, {11.15} planes)[51,59,60] indicate that the arrays are strongly textured with preferential orientation of the {015} and {205} planes perpendicular to the wire axis. Despite the lower signal intensity measured for the sample with a wire diameter of 130 nm electrodeposited in 60 μm PC membranes (red) in comparison to its counterpart in 30 μm membranes (orange), the relative intensity of the two observed peaks is similar for the two samples. The diffractograms further show that the smaller the nanowire diameter, the larger the ratio $I(015)/I(205)$ for samples fabricated at room temperature. For nanowire arrays with diameters below 30 nm, only the 015 reflection is measured. Assuming that there is no large variation in the nanowire length distribution in our set of samples, the ratio $I(015)/I(205)$ increases also with decreasing deposition temperature, which is influencing the ion transport to the cathode during the electrochemical growth process. The influence of temperature is visible by comparison of panels a and b in Figure 7. In Figure 7b, ω-2θ scans of wires grown at −100 mV vs SCE and 4 °C are presented. At lower temperatures, the nanowire arrays are also preferentially oriented with the {015} and {205} planes perpendicular to the nanowire axis. However, in the case of larger diameters (>30 nm), the ratio $I(015)/I(205)$ increases considerably. This change is more pronounced than shown in the work of Sander et al.,[28] where only a small change in the additional {300} peak was observed. The preferential orientation of crystallites within the nanowires is also modified by variation of the deposition potential. This is demonstrated in Figure 7c (0 mV, 20 °C) and Figure 7d (0 mV, 4 °C). The change in potential brings about the appearance of {110} and {101} reflections in arrays with larger wire diameters in both cases. The appearance of these two orientations and the absence of the 015 peak for depositions at more positive potentials are in agreement with previous results on thin films[61] and nanowires with a diameter of 200 nm.[33] For variation from −100 to 0 mV vs SCE for nanowires with diameters of 40−60 nm, the preferential orientation of the grains in the nanowires shifts from {015} and {205} planes to mostly {205} planes perpendicular to the wire axis. This is in excellent agreement with our TEM investigations on individual nanowires (Figures 5 and 6). Interestingly, with further reduction of the nanowire diameter below 30 nm, 015 peaks become dominant again.

These results demonstrate that electrodeposition in polymeric templates yields textured nanowire arrays with various preferential orientations and that it is possible to tune the preferred crystallographic orientation of nanowire arrays by varying the deposition potential for nanowires with both larger (120 nm) and smaller (50 nm) diameters. It further shows that the crystallographic orientation of the grains inside the nanowires not only depends on the electrochemical deposition conditions, that is, temperature, electrolyte, and potential, but also is influenced by either the diameter of the nanochannel or, as a consequence of the diameter variation, a change in the overall active area of deposition. The data in particular shows that, for selective changes in the preferential orientation in very thin nanowires (<30 nm) embedded in polymer membranes, deposition conditions need additional adjustment and parameters obtained from the growth of thin films or larger nanochannel diameters are not transferrable.

Influence of Electrolyte Concentration on Preferred Crystallographic Orientation. Figure 8 shows two ω-2θ diffractograms nanowire arrays that were deposited in 60 μm templates with a pore diameter of 120 nm and a pore density of 10^9/cm^2. The electrodeposition was conducted at 0 mV vs SCE at 20 °C, which allows for direct comparison with the results shown in Figure 7c for templates with 10^8 pores/cm^2 and pore diameters of 120−130 nm. As for deposition in 30 μm membranes, reflections from {101}, {110}, and {205} planes are visible. However, the signal intensity of the 205 reflection is significantly higher than in the other samples, underlining the existence of preferential growth with {205} planes perpendicular to the wire axis and suggesting that increased membrane thickness and/or larger active areas might be advantageous for

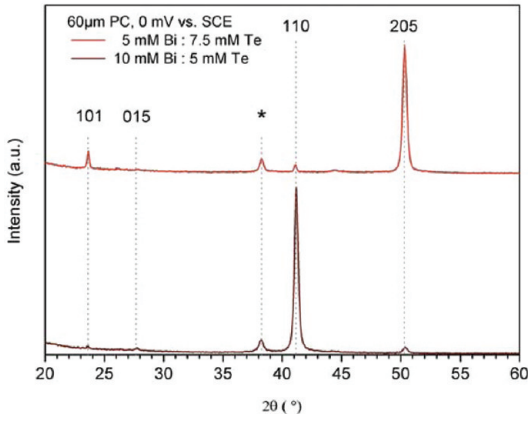

Figure 8. X-ray diffractograms of nanowire arrays embedded in 60 μm thick membranes, deposited at 0 mV vs SCE and 20 °C, using two electrolytes with different ion concentrations: 5 mM Bi and 7.5 mM Te (red) and 10 mM Bi and 5 mM Te (black). The asterisk (∗) corresponds to the reflection from the undissolved Au layer.

dx.doi.org/10.1021/jp210491g | J. Phys. Chem. C 2012, 116, 5367−5375

the preparation of nanowire arrays with enhanced texture. Thus, the influence of both parameters should be taken into account when studying the deposition process. In addition, in the case of longer nanowires grown in thicker templates, the concentration of the different components may vary along the nanowires, as indicated by Wang et al.,[33] and thus should be also carefully analyzed. To exemplarily demonstrate the influence of the electrolyte and the possibility of obtaining a third preferential growth direction in PC membranes, that is, next to alignment of the {205} and {015} planes perpendicular to the wire axis, we include the diffractogram of a sample grown from a Bi-rich electrolyte, while all other parameters for synthesis, that is, membrane properties and electrodeposition conditions, were kept fixed. Under these conditions, it is possible to electrochemically grow a nanowire array at 0 mV vs SCE with preferential growth of {110} planes perpendicular to the nanowire axis. These results open up the possibility to investigate the thermoelectric properties of nanowires with the same size and three different preferential crystalline orientations.

CONCLUSIONS

We demonstrate the electrodeposition of Bi_2Te_3 nanowires in etched ion-track membranes with thicknesses of 10, 30, and 60 μm. Specific membranes have been fabricated at GSI by heavy-ion irradiation and chemical etching, to facilitate the growth of both, very thin nanowires with average diameters close to 10 nm, as well as long wires with average diameters around 130 nm and maximum lengths of 60 μm. Our systematic studies demonstrate the influence of deposition temperature and voltage influence on the growth conditions and, thus, the resulting surface morphology and crystallographic orientation of nanowires. Furthermore, TEM/EDS showed that nanowires deposited at 0 mV vs SCE are close to the stoichiometric composition of Bi_2Te_3. While TEM and XRD analyses show that the nanowires are polycrystalline, their preferential crystallographic orientation is adjustable by deposition potential, temperature, and electrolyte concentration. Our results show that the versatility of electrochemical deposition in ion-track etched membranes can be an asset to the formation of well-controlled thermoelectric model systems and improve the basic understanding of template-assisted nanowire growth.

AUTHOR INFORMATION

Corresponding Author

*E-mail: o.picht@gsi.de (O.P.), m.e.toimilmolares@gsi.de (M.E.T.-M.).

Notes

The authors declare no competing financial interest.

ACKNOWLEDGMENTS

We thank the Deutsche Forschungsgemeinschaft (DFG) within the SPP 1386 for financial support. The authors thank J. Brötz for helpful advice during the first XRD investigations. Sandia National Laboratories is a multiprogram laboratory managed and operated by Sandia Corporation, a wholly owned subsidiary of Lockheed Martin Corporation, for the U.S. Department of Energy's National Nuclear Security Administration under Contract DE-AC04-94AL85000. Support for D.L.M. and J.L.-F. was provided, in part, by the Sandia LDRD Office.

REFERENCES

(1) Rowe, D. M., Ed. *Thermoelectrics Handbook: Macro to Nano*; Taylor & Francis: New York, 2006.
(2) Hicks, L. D.; Dresselhaus, M. S. *Phys. Rev. B* **1993**, *47*, 12727–12731.
(3) Hicks, L. D.; Dresselhaus, M. S. *Phys. Rev. B* **1993**, *47*, 16631–16634.
(4) Singh, M. P.; Bhandari, C. M. *Solid State Commun.* **2003**, *127*, 649–654.
(5) Balandin, A.; Wang, K. L. *J. Appl. Phys.* **1998**, *84*, 6149–6153.
(6) Bejenari, I.; Kantser, V. *Phys. Rev. B* **2008**, *78*, 115322.
(7) Bejenari, I.; Kantser, V.; Balandin, A. A. *Phys. Rev. B* **2011**, *81*, 075316.
(8) Qiu, B.; Sun, L.; Ruan, X. *Phys. Rev. B* **2011**, *83*, 035312.
(9) Venkatasubramanian, R.; Siivola, E.; Colitts, T.; O'Quinn, B. *Nature* **2001**, *413*, 597–602.
(10) Poudel, B.; Hao, Q.; Ma, Y.; Lan, Y.; Minnich, A.; Yu, B.; Yan, X.; Wang, D.; Muto, A.; Vashaee, D.; Chen, X.; Liu, J.; Dresselhaus, M. S.; Chen, G.; Ren, Z. *Science* **2008**, *320*, 634–638.
(11) Ma, Y.; Hao, Q.; Poudel, B.; Lan, Y.; Yu, B.; Wang, D.; Chen, G.; Ren, Z. *Nano Lett.* **2008**, *8*, 2580–2584.
(12) Tang, X.; Xie, W.; Li, H.; Zhao, W.; Zhang, Q.; Niino, M. *Appl. Phys. Lett.* **2007**, *90*, 012102.
(13) Fan, S.; Zhao, Z.; Yan, Q.; Ma, J.; HNG, H. H. *J. Electron. Mater.* **2011**, *40*, 1018–1023.
(14) Zhang, Y.; Wang, H.; Krämer, S.; Shi, Y.; Zhang, F.; Snedaker, M.; Ding, K.; Moskovits, M.; Snyder, G. J.; Stucky, G. D. *ACS Nano* **2011**, *5*, 3158–3165.
(15) Zhou, J.; Jin, C.; Seol, J. H.; Li, X.; Shi, L. *Appl. Phys. Lett.* **2005**, *87*, 133109.
(16) Mavrokefalos, A.; Moore, A. L.; Pettes, M. T.; Shi, L.; Wang, W.; Li, X. *J. Appl. Phys.* **2009**, *105*, 104318.
(17) Hochbaum, A. I.; Chen, R.; Delgado, R. D.; Liang, W.; Garnett, E. C.; Najarian, M.; Majumdar, A.; Yang, P. *Nature* **2008**, *451*, 163–167.
(18) Boukai, A. I.; Bunimovich, Y.; Tahir-Kheli, J.; Yu, J.-K.; Goddard, W. A. III; Heath, J. R. *Nature* **2008**, *451*, 168–171.
(19) Borca-Tasciuc, D.-A.; Chen, G.; Prieto, A.; Martín-González, M. S.; Stacy, A.; Sands, T.; Ryan, M. A.; Fleurial, J. P. *Appl. Phys. Lett.* **2004**, *85*, 6001–6003.
(20) Biswas, K. G.; Sands, T. D.; Cola, B. A.; Xu, X. *Appl. Phys. Lett.* **2009**, *94*, 223116.
(21) Venkatasubramanian, R.; Colpitts, T.; O'Quinn, B.; Liu, S.; El-Masry, N.; Lamvik, M. *Appl. Phys. Lett.* **1999**, *75*, 1104–1106.
(22) Wang, W.; Goebl, J.; He, L.; Aloni, S.; Hu, Y.; Zhen, L.; Yin, Y. *J. Am. Chem. Soc.* **2010**, *132*, 17316–17324.
(23) Deng, Y.; Nan, C.-W.; Wei, G.-D.; Guo, L.; Lin, Y.-H. *Chem. Phys. Lett.* **2003**, *374*, 410–415.
(24) Yu, H.; Gibbons, P. C.; Buhro, W. E. *J. Mater. Chem.* **2004**, *14*, 595–602.
(25) Purkayastha, A.; Lupo, F.; Kim, S.; Borca-Tasciuc, T.; Ramanath, G. *Adv. Mater.* **2006**, *18*, 496–500.
(26) Ham, J.; Shim, W.; Kim, D. H.; Lee, S.; Roh, J.; Sohn, S. W.; Oh, K. H.; Voorhees, P. W.; Lee, W. *Nano Lett.* **2009**, *9*, 2867–2872.
(27) Prieto, A. L.; Sander, M. S.; Martín-González, M. S.; Gronsky, R.; Sands, T.; Stacy, A. M. *J. Am. Chem. Soc.* **2001**, *123*, 7160–7161.
(28) Sander, M. S.; Gronsky, R.; Sands, T.; Stacy, A. M. *Chem. Mater.* **2003**, *15*, 335–339.
(29) Jin, C.; Xiang, X.; Jia, C.; Liu, W.; Cai, W.; Yao, L.; Li, X. *J. Phys. Chem. B* **2004**, *108*, 1844–1847.
(30) Wang, W.; Huang, Q.; Jia, F.; Zhu, J. *J. Appl. Phys.* **2004**, *96*, 615–618.
(31) Menke, E. J.; Li, Q.; Penner, R. M. *Nano Lett.* **2004**, *4*, 2009–2014.
(32) Li, L.; Yang, Y.; Huang, X.; Li, G.; Zhang, L. *Nanotechnology* **2006**, *17*, 1706–1712.
(33) Wang, W.-L.; Wan, C.-C.; Wang, Y.-Y. *J. Phys. Chem. B* **2006**, *110*, 12974–12980.

(34) Trahey, L.; Becker, C. R.; Stacy, A. M. *Nano Lett.* **2007**, *7*, 2535−2539.
(35) Lee, J.; Farhangfar, S.; Lee, J.; Cagnon, L.; Scholz, R.; Gösele, U.; Nielsch, K. *Nanotechnology* **2008**, *19*, 365701.
(36) Chen, C.-L.; Chen, Y.-Y.; Lin, S.-J.; Ho, J. C.; Lee, P.-C.; Chen, C.-D.; Harutyunyan, S. R. *J. Phys. Chem. C* **2010**, *114*, 3385−3389.
(37) Xiao, F.; Yoo, B.; Lee, K.-H.; Myung, N. V. *Nanotechnology* **2007**, *18*, 335203.
(38) Apel, P. Yu.; Blonskaya, I. V.; Orelovich, O. L.; Akimenko, S. N.; Sartowska, B.; Dmitriev, S. N. *Colloid J.* **2004**, *66*, 649−656.
(39) Schönenberger, C.; van der Zande, B. M. I.; Fokkink, L. G. J.; Henny, M.; Schmid, C.; Krüger, M.; Bachtold, A.; Huber, R.; Birk, H.; Staufer, U. *J. Phys. Chem. B* **1997**, *101*, 5497−5505.
(40) Koukharenko, E.; Li, X.; Nandhakumar, I.; Frety, N.; Beeby, S. P.; Cox, D.; Tuder, M. J.; Schiedt, B.; Trautmann, C.; Bertsch, A.; White, N. M. *J. Micromech. Microeng.* **2008**, *18*, 104015.
(41) Frantz, C.; Stein, N.; Gravier, L.; Granville, S.; Boulanger, C. *J. Electron. Mater.* **2009**, *39*, 2043−2048.
(42) Wang, W.; Jia, F.; Huang, Q.; Zhang, J. *Microelectron. Eng.* **2005**, *77*, 223−229.
(43) Keyani, J.; Stacy, A. M.; Sharp, J. *Appl. Phys. Lett.* **2006**, *89*, 233106.
(44) *Datasheet Makrofol KG*; Mobay Chemical Corporation: Pittsburgh, PA.
(45) Cornelius, T. W.; Schiedt, B.; Severin, D.; Pépy, G.; Toulemonde, M.; Apel, P. Yu.; Boesecke, P.; Trautmann, C. *Nanotechnology* **2010**, *21*, 155702.
(46) Magri, P.; Boulanger, C.; Lecuire, J.-M. *J. Mater. Chem.* **1996**, *6*, 773−779.
(47) Toimil Molares, M. E.; Balogh, A. G.; Cornelius, T. W.; Neumann, R.; Trautmann, C. *Appl. Phys. Lett.* **2004**, *85*, 5337−5339.
(48) Toimil Molares, M. E.; Buschmann, V.; Dobrev, D.; Neumann, R.; Scholz, R.; Schuchert, I. U.; Vetter, J. *Adv. Mater.* **2001**, *13*, 62−65.
(49) Fleurial, J.; Gailliard, L.; Triboulet, R.; Scherrer, H.; Scherrer, S. *J. Phys. Chem. Solids* **1988**, *49*, 1237−1247.
(50) Nakajima, S. *J. Phys. Chem. Solids* **1963**, *24*, 479−485.
(51) Francombe, M. H. *Br. J. Appl. Phys.* **1958**, *9*, 415−417.
(52) Wiese, J. R.; Muldawer, L. *J. Phys. Chem. Solids* **1960**, *15*, 13−16.
(53) Lin, Y.-M.; Sun, X.; Dresselhaus, M. S. *Phys. Rev. B* **2000**, *62*, 4610−4623.
(54) Lan, Y.; Poudel, B.; Ma, Y.; Wang, D.; Dresselhaus, M. S.; Chen, G.; Ren, Z. *Nano Lett.* **2009**, *9*, 1419−1422.
(55) Yan, X.; Poudel, B.; Ma, Y.; Liu, W. S.; Joshi, G.; Wang, H.; Lan, Y.; Wang, D.; Chen, G.; Ren, Z. F. *Nano Lett.* **2010**, *10*, 3373−3378.
(56) Cornelius, T. W.; Toimil Molares, M. E.; Neumann, R.; Karim, S. *J. Appl. Phys.* **2006**, *100*, 114307.
(57) Karim, S.; Ensinger, W.; Cornelius, T. W.; Neumann, R. *Physica E* **2008**, *40*, 3173−3178.
(58) Steinhögl, W.; Schindler, G.; Steiniesberger, G.; Engelhardt, M. *Phys. Rev. B* **2002**, *66*, 075414.
(59) X-ray standard powder diffraction pattern: JCPDS 15-0863.
(60) X-ray standard powder diffraction pattern: JCPDS 82-0358.
(61) Miyazaki, Y.; Kajitani, T. *J. Cryst. Growth* **2001**, *229*, 542−546.